https://doi.org/10.5194/tc-2022-144
Preprint. Discussion started: 21 July 2022

The Cryosphere Discussions
Open Access
EGU

Drainage and refill of an Antarctic Peninsula subglacial lake reveals an active subglacial hydrological network

Dominic A. Hodgson[1], Tom A. Jordan[1], Teal R. Riley[1], Peter T. Fretwell[1]

[1]British Antarctic Survey, High Cross, Madingley Road, Cambridge CB3 0ET, UK

Correspondence to: Dominic A Hodgson (daho@bas.ac.uk)

Abstract. The role of subglacial hydrological networks and subglacial lakes in modulating ice dynamics under the East and West Antarctic Ice Sheets is now relatively well understood. In contrast, little is known about subglacial water bodies under the Antarctic Peninsula Ice Sheet and how these are influencing glacier behaviour. Here we describe the rapid drainage and slow refill of a subglacial lake under Mars Glacier using remote sensing and aerogeophysics platforms. Results suggest drainage of the subglacial lake occurred prior to 2013, resulting in collapse of the overlying ice into the newly formed subglacial cavity. The lake has been refiling since this time, with peak rates of infilling associated with seasonal meltwater activity. We review evidence for similar features elsewhere in the Antarctic Peninsula and discuss whether their appearance marks a threshold shift in the thermal regime of the region's glaciers and the activation of their subglacial hydrological networks. Collectively, these features show coupling of surface climate processes and the bed and may help explain the strong seasonality seen in glacier flow rates during the annual melt season and the ongoing regional decline in ice mass.

1 Introduction

Changes in glacial and subglacial hydrology can result in significant impacts on glacier and ice sheet dynamics including accelerating ice flow (Bartholomew et al., 2012). Active subglacial hydrological networks have been revealed from changes in ice surface elevation detected by airborne radio-echo sounding and satellite altimetry (Livingstone et al., 2022), and overland seismic surveys have been used to detect water column, sediment properties and overlying ice sheet behaviour in subglacial lakes (Smith et al., 2018). Much of this work has been carried out on large subglacial lakes under the East and West Antarctic Ice Sheets, while small lakes under the valley glaciers of the Antarctic Peninsula Ice Sheet have received comparatively little attention (cf. the study of Alaskan alpine subglacial lakes by Capps et al., 2010). In a recent global inventory of subglacial lakes, only one is included on the Antarctic Peninsula (Livingstone et al., 2022) beneath Crane Glacier in northeast Graham Land (Scambos et al., 2011), and another has previously been described and directly sampled on Alexander Island (Hodgson et al., 2009a; Hodgson et al., 2009b; Pearce et al., 2013).

Rapid warming of the Antarctic Peninsula region over the last five decades had led to its ice caps and valley glaciers losing mass at an average rate of 24 Gt yr^{-1}, contributing 2.5 ± 0.4 mm sea-level rise since 1979 (Rignot et al., 2019). Associated with this mass loss there has been widespread accumulation of seasonal surface meltwater, which models predict will double in volume by 2050 (Trusel et al., 2015). This meltwater is particularly prevalent at lower altitudes, for example on ice shelves, in glacier ablation zones, and at the edges of glaciers where proximity to overland meltwater, increased radiative melt from low albedo rock outcrops, and the

https://doi.org/10.5194/tc-2022-144
Preprint. Discussion started: 21 July 2022

supply of surface dust all act to increase meltwater volume. Seasonal meltwater lakes are now common on the surface of many ice shelves and at the shear zones of their feeder glaciers (Fig. 1 c and d). In some years, sustained positive air temperatures have resulted in exceptional iceshelf meltwater accumulations (Banwell et al., 2021). This water refreezes in winter, percolates into fractures, or drains into the underlying ocean through moulins or ice dolines (cf. Bindschadler et al., 2002; Lenaerts et al., 2017; Warner et al., 2021). Collectively these processes have contributed to ice shelf collapse due to meltwater driven fracture (Lai et al., 2020).

Whilst the presence of seasonal meltwater on Antarctic Peninsula ice shelves is well-documented and monitored, the role of water on the surface, within and at the base of the region's glaciers is less well studied (Tuckett et al., 2019) which limits our understanding of regional glacier dynamics. In this paper we use remote sensing and aerogeophysics data to describe the catastrophic drainage of a subglacial lake under Mars Glacier on Alexander Island which caused collapse of the overlying ice into a subglacial cavity. We review evidence for similar features elsewhere in the Antarctic Peninsula and Antarctica and discuss whether their appearance marks a shift in the thermal regime of (some) Antarctic glaciers and the activation of their subglacial hydrological networks.

1.1 Site description

The main study site is an ice depression located on the western side of Mars Glacier, south-eastern Alexander Island (71°51'01''S, 68°28'36''W) (Figs 1 and 2). The depression is situated within a broader cirque occupied by ice, snow, and bedrock outcrops at the northern end of Phobos Ridge. It appears to be the result of a vertical collapse of the ice surface, and we refer to it here as the Phobos Ice Collapse Structure (PICS). The adjacent Mars Glacier is 15 km long and 3-4 km wide and lies between Two Step Cliffs and Phobos Ridge. It feeds into Saturn Glacier which discharges into George VI Ice Shelf across an ice shelf shear zone (Fig. 1b). Phobos Ridge consists of sandstones and shales and has three small west-east oriented ice filled valleys or cirques which are part of Mars Glacier. The study site is in the northernmost valley, situated at an altitude of c. 270 m. This valley has an enclosed surface hydrological catchment draining into the PICS with an area of 1.36 km^2.

2. Methods

The PICS site cannot easily be accessed overland so all analyses were based on remote sensing (cf. Warner et al., 2021). Initial characterisation was carried out using oblique aerial photographs taken from a British Antarctic Survey (BAS), DeHaviland Twin Otter aircraft in December 2018 (Fig. 2). Subsequent detailed assesment of the site was made during two overflights by the BAS aerogeophysical equipped Twin Otter VP-FBL on the 22nd and 30th December 2019 during transits to and from survey tasking for the International Thwaites Glacier Collaboration (ITGC).

The survey aircraft was equiped with a Riegl Q240i scanning LiDAR. The LiDAR data were processed by Terratec, who intergrated the raw scanning LiDAR data, GNSS positional data and INS attitude data, and carried out boresight calibration based on repeat passes over Rothera Research Station on Adelaide Island (67°34′06″S 68°07′33″W). The resulting point cloud provides acurate measurements of surface elevation (~10 cm standard deviation) across the study area (Fig. 3a and b). In our study area the aircraft survey altitude meant

https://doi.org/10.5194/tc-2022-144
Preprint. Discussion started: 21 July 2022

that a point density of 0.2 to 0.4 points per m^2 was achieved. This elevation dataset provides a very high resolution snapshot of the local geomorphology and reveals how it changed during the short (8 day) period between overflights.

In addition to raw elevation values the LiDAR also returns a parameter describing the strength of the LiDAR reflection at every point, known as the intensity (Kashani et al., 2015). We carried out two simple adjustments to the raw intensity values: First, we corrected for the reduction in intensity due to the scan angle by fitting a 2^{nd} order polynomial to a plot of scan angle vs intensity over a local area of aproximately flat white snow. Second, the amplitude was normalised to simplify comparison between the two flights. These corrections were not rigorously calibrated between flights, and additional correction for range to ground and aircraft attitude could be carried out. However, the general pattern of intensity with these basic adjustments provides usefull data (Fig. 3c and d), with low intensity returns reflecting rough or wet regions, while higher intensity returns indicate a simple and more reflective surface (Kashani et al., 2015).

To asses the geomorphology and structure of the subglacial bed we utilised data from the Cresis 600-900 MHz accumulation radar (Arnold, 2020). This radar system was mounted on the BAS aerogeophysical survey aircraft during the December 2019 survey flights, and collected data simultaneously with the LiDAR. The data from the accumulation radar has a long track resolution of 20 to 30 m, depending on aircraft spead and a depth resolution on the order of 50 cm (Arnold, 2020). Data shows the amplitude of the radar reflections, on a log scale. The range is calculated from radar two-way travel time in ice. Variations in aircraft elevation and range to surface will induce some distortion to the images, but the relative depth of englacial structures beneath the ice surface is robust.

Longer term changes in the surface elevation of the site were determined from the Reference Elevation Model of Antarctica (REMA; https://www.pgc.umn.edu/data/rema/) using data from 2013 to 2017 (Howat et al., 2019). REMA is a high resolution, time-stamped Digital Elevation Model (DEM) of Antarctica at 8-meter spatial resolution. The provided REMA dataset includes both an average mosaic DEM assembled from multiple strip DEMs and the underlying time-stamped 'strip' files. The strip files were generated by applying fully automated, stereo auto-correlation techniques to overlapping pairs of high-resolution optical satellite images, using the open source Surface Extraction from TIN-based Searchspace Minimization (SETSM) software (Howat et al., 2019). The strip files are not registered to satellite altimetry, meaning that although relative elevation within a strip is robust they have lower absolute accuracy. To counter this issue, and allow assesment of long term local changes in elevation, we assumed a fixed surface elevation outside the proposed collapse feature based on the airborne LiDAR reference. In our study area elevation strips were available for 2013/09/12, 2014/02/10, 2016/02/14 and 2017/01/17.

3. Results

3.1 Aerial photographs and regional setting

Oblique aerial photographs show a collapsed ~280 by 350 m depression in the glacier surface bounded by almost shear ice cliffs (Fig. 2). Ice cliffs on the southern side of the PICS have multiple incisions formed by

https://doi.org/10.5194/tc-2022-144
Preprint. Discussion started: 21 July 2022

surface meltwater steams, active at the time of image acquisition (3rd Dec 2018) (Fig. 2b). There is also a substantial block of ice calving off the ice cliff, forming a new cliff face (Fig 2b). Drifting snow towards Mars Glacier has partially obscured the cliffs on the northern side. There are several concentric bridged crevasses oriented towards the PICS visible on the snow surface on the northern side. A number of horizontal dust layers can be seen within the ice cliff face. Supraglacial rock debris is present on the snow surface to the southwest.

3.2 LiDAR geomorphology and reflectivity

The 2019 LiDAR data show the PICS floor sitting at an altitude of ~245 m, compared to the surrounding ice surface, which has an elevation of >270 m (Fig 3a), indicating the PICS is currently ~25 m deep. The area of the PICS, enclosed by the ice cliffs, is 0.067 km^2. The PICS floor is approximately flat, with an assortment of ~ 2-3 m topographic highs present towards the centre of the basin. The deepest values (243.5 to 244 m) are adjacent to the PICS walls, forming an internal 'moat' around the floor. The PICS walls tend to be steepest to the south and west, with the 20 m high, block calving from the southern ice cliffs clearly resolved (Fig. 3a and b). The detailed structures within the PICS were generally consistent between the two flights (Fig. 3a and b). Extending southward from the PICS rim an approximately 100 m wide 10 m deep (between 260 and 270 m attitude) catchment depression was imaged on the 22nd of December flight (Fig. 3a). This region is not well imaged by the 30th of December flight (Fig. 3b), despite elevation values being recovered at similar angles from the centre-line further along the LiDAR swath.

The LiDAR reflectivity shows high values around the northern rim of the caldera in both LiDAR flights (Fig. 3c and d). South of the PICS there is an area of low reflectivity on the 22nd of December flight broadly corresponding with the catchment depression noted in the topography, although the low reflectivity zone continues further south following the base of a valley indicated by the shading of the topography (Fig. 3a). On the 30th of December flight the previously low reflectivity area returns very few surface elevation observations, and the area of low reflectivity has expanded along the entire southern margin of the PICS (Fig. 3d). The area of low/absent reflectivity corresponds to the area marked by numerous supra-glacial streams flowing over the PICS wall in the aerial photographs and is likely due to a high and increasing amount of melt water in this area between overflights. The patches of distinct high and low reflectivity with abrupt linear edges south of the PICS on the 30th December flight mark areas of rock exposure (Fig. 3d).

3.3 Subsurface geomorphology

Radar transects flown in orthogonal directions across the depression show significant clutter likely associated with off axis reflections and multiple reflections between the aircraft and the ice surface (Fig. 4). However, shallow reflectors 35-50 m below the ice surface indicate the PICS lies in a broad topographic bowl (Fig. 4b). However, a significant bedrock dam is not imaged on the down-glacier side of the PICS (Fig. 4d). Bright reflectors at depths of 10-20 m directly beneath the PICS, are hard to interpret and may be due to the ice sheet bed, en-glacial water, or off axis reflectors. The base of the adjacent Mars Glacier trunk can be imaged beneath ~400 m of ice (Fig. 4a, 4c).

3.4 Surface elevation changes

https://doi.org/10.5194/tc-2022-144
Preprint. Discussion started: 21 July 2022

The REMA surface elevation measurements from 2013, 2014, 2016, 2017, and LiDAR Dec 22nd 2019 and Dec 30th 2019 show that the PICS has undergone dynamic surface elevation changes (Figs. 3 and 5). It was present, at or before 2013, with a maximum observed depth of ~44 m and a volume of ~2,796,000 m^3 (Fig. 5a). Since 2013 the floor of the PICS has been rising in all surveyed years, with~1,405,000 m^3 of material filling the PICS between 2013 and 2019. We interpret this as refilling of the subglacial cavity, rather than the accumulation of blowing snow which is focused on the northern side (Fig. 2). The closely spaced LiDAR observations on 22nd and 30th December 2019 show the PICS floor rose by ~1.18 m; equivalent to ~71,000 m^3 of meltwater input in just 8 days. As the PICS floor rose by ~1.18 m the surrounding area fell by 10 to over 80 cm (Fig. 6), with most extreme elevation changes on steep slopes to the south, including areas incised by surface meltwater steams which were flowing into PICS via waterfalls when the aerial photographs were taken. Local melting, if spread across the catchment, could account for a large part of the observed increase in surface elevation within the feature. This would require ~7 cm of surface melt across the local catchment in 8 days.

Cross sections of surface elevation changes in the depression (marked by blue lines in Fig. 6 and shown in Fig 7), show the infilling since 2013. The N-S line shows the development of the drifting snow infill on the northern side of the depression and the collapse of the ice cliff on the southern side forming an ice block between the 2017 REMA and the 2019 LiDAR surveys, which has become detached and sunk into the depression. The W-E line also shows the snow infill on the northern side of the depression and the continued retreat and steepening of the ice cliffs to the west. It also crosses one of the raised features in the depression which are 2-3 m above the basin floor. A plot of the mean elevation change extracted from the two profiles crossing the basin shows a more or less linear decrease in basin depth of 3.28 ma^{-1} (Fig. 8). The substantially higher 1.18m elevation increase, recorded between the 22nd and 30th December LiDAR surveys equates to a short-lived infill rate of 53 ma^{-1}.

4. Discussion

Collectively, the evidence presented here is consistent with the catastrophic drainage of a subglacial lake, and collapse of the overlying ice sometime before 2013. The radar transects identify a broad bedrock depression in orthogonal transects which could retain subglacial water. However, the dam sealing the depression must be a transient glacial feature, to allow for significant drainage followed by the progressive and long-term re-filling. This is consistent with the along flow radar profile (Fig. 4d), which does not image a major topographic dam on the downstream side of the PICS.

The catastrophic nature of the drainage event is supported by the presence of the steep bounding ice cliffs which suggest loss of hydraulic support for the overlying ice and its collapse into a subsurface void following rapid drainage of the subglacial lake. This process is seen at a smaller scale between the 2017 REMA and the 2019 LiDAR surveys with the detachment of a block of ice, and formation of a new ice cliff on the southern side of the depression, and the concentric crevasses which mark similar ongoing, or partial, structural failures of the ice on the northern side (Fig. 2). The lake occupying the subglacial cavity must be at least 46 m deep, using the maximum height of the ice cliffs in 2013 as a proxy for water depth. The depth of the ice column between the surface depression and the underlying rock cavity is unknown. The topography at the base of the PICS appears relatively rugged in 2013, but was flatter in subsequent years (Fig. 5 and 7). This suggests that either that

https://doi.org/10.5194/tc-2022-144
Preprint. Discussion started: 21 July 2022

drainage may have been complete, allowing the basal topography to show through, or that the features are fragments of collapsed ice cliff, or ice blisters (Moore, 1993). The very flat floor of the PICS in subsequent years would be consistent with progressive filling of the cavity, and floatation of ice off the bed, or the melting or incorporation of these features.

As the subglacial basin is not constrained by a significant topographic bedrock dam, its rapid drainage is consistent with the failure of a grounded ice dam at its lowest point, with water able to break though the seal and escape beneath the glacier. This could occur as a result of water level or pressure increases in the cavity exerting hydrostatic pressure on the ice, or floatation of ice at an ice dam breaking contact with the bed triggering drainage. Glen (1954) recognised from glacier lake drainage events in British Columbia, that this process can be asymmetric, with enlargement of the lake under the ice in the downhill direction causing increased pressure there relative to the other points, the opening of conduits to the subglacial hydrological network, and catastrophic emptying. Subglacial lake outburst flood models refer to this as 'superflotation water pressures' where excess water pressure exceeds the ice overburden pressure and drives water along the ice–bed interface, creating conduits linking into pre-existing subglacial drainage paths (Clarke, 2003). In the case of PICS the flotation of the ice dam may have been enhanced by increased inputs from surface melt in the catchment (this processs has been described in volcanic and hydrothermal systems in Iceland, Björnsson, 2003). As with conceptual models of (subaerial) glacial lake outburst floods, frictional heat dissipated by the escaping water can enlarge subglacial conduits allowing continued drainage (P. 92, Benn and Evans, 2010). In this model, eventually water pressure falls to the extent that closure of the conduit by ice creep exceeds melting rates and the seal is reformed allowing the lake to refill. If this mechanism is correct, we can assume that full, or at least partial resealing had occurred by 2013. This pattern of rapid drainage and slow recharge has been described in some Greenland lakes (Livingstone et al., 2019).

Subsequent seasonal inputs of meltwater from the catchment, glacier surface and likely seepage through porous firn or a linked cavity network has gradually refilled the basin, raising its surface by ~ 30 m in six years. The 1.18 m increase in the surface elevation between 22nd and 30th December 2019 substantially exceeds the overall infill trend, confirming the seasonality of meltwater inputs, and coincides with the 32-year record-high surface melt in 2019/2020 recorded on the northern George VI Ice Shelf (Banwell et al., 2021). The relative contributions of surface meltwater and englacial hydrological processes to the long-term refilling are not known.

Overall, the feature conforms to Livingstone et al's. descriptions of 'water-filled cavities that drain rapidly beneath valley glaciers' (Fig. 7c in Livingstone et al., 2022). However, circular ice depressions, referred to as 'ice cauldrons' (or 'ice caldera') have also been recognised in areas of volcanic or geothermal activity, for example in Iceland (e.g. Reynolds et al., 2019). Volcanic 'ice cauldrons' are caused by ice melting at their base and are likely to be linked to minor subglacial eruptions and often occur in clusters that may trace the caldera margin, dyke or rift features. We consider a volcanic origin unlikely for the PICS. There is no evidence of local volcanism around Phobos Ridge or Mars Glacier, although the Beethoven Peninsula volcanic field (Fig. 1a) may extend towards the south eastern margins of Alexander Island (Smellie and Hole, 2021). Late Neogene post-subduction volcanism has been identified elsewhere on Alexander Island and southwest Palmer Land, likely related to the ascent and decompressional melting of mantle through slab windows. This encompasses widely scattered and isolated outcrops of the Late Neogene Bellingshausen Sea Volcanic Group between 8 – 2.5 Ma

https://doi.org/10.5194/tc-2022-144
Preprint. Discussion started: 21 July 2022

(Smellie et al., 1988). Thermal wavelength imagery of 700,000 year old volcanic rocks at Gluck Peak (148 km west) indicate elevated heat flow, which may be attributable to ongoing geothermal activity in Alexander Island (Smellie and Hole, 2021), although no primary volcanic landforms have been identified.

4.1 Evidence elsewhere

The feature described here is not unique. At the north eastern end of the Antarctic Peninsula in Graham Land, adjacent to the Sjögren Glacier (64°12'S, 58°58'W) a 380 m diameter, 35 m deep circular depression was first described in 1957 (referred to as an 'ice caldera', but with no link to volcanic activity; Aitkenhead, 1963) (Figs. 1 and 9). Its formation was linked to an abundance of seasonal meltwater resulting from föhn winds. Subsequent observations showed a rapid lake drainage event, presumably via a subglacial channel, between June 1961 and 2 August 1961 following a period of 'unusually warm temperature' resulting in a collapse of the overlying ice by c. 20 m. A similar but smaller feature (50 x 30 m) was also described from Hope Bay at Nobby Nunatak (Koerner, 1964); an area which has now recorded the highest confirmed temperatures in Antarctica of 18.3°C (Francelino et al., 2021). More recently in March 2022, an analogous feature was photographed 92 km North of PICS at Callisto Cliffs (Alexander Island; 71° 01' S., 68° 20' W) with characteristics consistent with drainage of another subglacial water body and collapse of the overlying ice (Fig. 10). Elsewhere, a 183 m × 220 m depression bounded by ice cliffs has been described in the Larsemann Hills, East Antarctica; although in this case the collapse of the overlying ice was caused by drainage of supraglacial water and nearby epiglacial lakes into an englacial cavity in 2017 causing its overfill and outburst (Boronina et al., 2021).

4.2 Wider implications

Our hypothesis is that these relatively rare subglacial lake drainage events, and the resulting ice collapse features, mark a threshold in the development of polythermal glacier behaviour. They appear to predate the formation of supraglacial lakes (at similar altitudes on the Antarctic Peninsula), providing a first surface expression of changing glacier basal hydrology in areas of regional warming. The 'ice caldera' in Graham Land was first described in the late 1950's at the onset of regional warming of the north-eastern Antarctic Peninsula (data from Esperanza Station shown in Turner et al., 2016) and following the regional intensification of the Southern Hemisphere Westerly Winds from the 1920's (Perren et al., 2020) which likely increased the frequency of the föhn winds that cause rapid surface melt events in northeast Graham Land (Laffin et al., 2021). Re-examination of this feature in Google Earth images from 2015 (Fig. 9b) show the rocky lake floor is now fully exposed, the overlying ice has gone, the surrounding catchment is extensively deglaciated with bounding glaciers heavily crevassed and fragmented and Prince Gustav Channel Ice Shelf which they formerly discharged has disappeared (Cooper, 1997). It can now be reclassified as an ice marginal lake (cf. Carrivick et al., 2022).

The apparent recent appearance of similar features 926 km further south on Alexander Island at the PICS and Callisto Cliffs may indicate the southward expression of this phase of glacier response to regional warming (at or before 2013). At the same time, analysis of flow rates of glaciers feeding George VI Ice Shelf have shown a c. 15% mean acceleration of, relative to their time-averaged baselines (Boxall et al., 2022), consistent with the activation of their subglacial hydrological networks. Similar accelerations have been described in Icelandic glaciers following subglacial floods (Magnússon et al., 2007). The presumed catastrophic nature of the PICS

https://doi.org/10.5194/tc-2022-144
Preprint. Discussion started: 21 July 2022

drainage prior to 2013, and slow subsequent re-filling of the subglacial cavity, also highlights the fact that subglacial hydrological processes can introduce significant non-linear feedbacks into the Antarctic Peninsula glacial system, with a time scale of years to decades.

The identification of active subglacial hydrological networks as far south as southern Alexander Island suggests a coupling of surface climate processes and the bed, and helps explain the strong seasonality seen in glacier flow rates during the annual melt season (Boxall et al., 2022). This can be attributed to an increase in basal water pressure, enhancing basal motion (Tuckett et al., 2019) and increased coupling between supraglacial and basal hydrology. As meltwater seasons are extended under future + 3°C climate change scenarios (Deconto et al., 2021), enhanced subglacial hydrological activity and acceleration in ice flow can be anticipated for longer periods, speeding up the deglaciation of the Antarctic Peninsula Ice Sheet.

5. Conclusions

Our detailed analysis of the changing geometry of a ~ 250 m wide circular, steep-sided depression in the surface of Mars Glacier is consisent with the drainage of a subglacial lake and the collapse of the overlying ice. The collapse structure formed in or prior to 2013, and has been re-filling ever since, reducing its depth from 45 to 25 m. Although the long-term filling trend is approximately linear, repeat LiDAR observations separated by just 8 days show the basin floor rose by ~1.18 m, equating to ~71,000 m^3 of meltwater input from a catchment just 1.36 km^2. This coincides with the 32-year record-high surface melt in 2019/2020 recorded on the northern George VI Ice Shelf and regional evidence of strong seasonality on glacier flow rates. This suggests that the subglacial hydrological networks in this region are immediately responding to changes in surface climate. As subglacial hydrological networks have been linked to changes in glacier flow and grounding line retreat, this close coupling between the surface and the bed of the region's glaciers shows their ongoing vulnerability to climate change.

Data availability. The datasets used in this paper are available at the NERC Polar Data Centre (http://www.bas.ac.uk/data/uk-pdc/)

Competing interests. The authors have no conflict of interest.

Author contributions. DAH and TAJ contibuted equally to this paper. DAH conceived the study from initial aerial photography supplied by BAS pilots. TAJ carried out the remote sensing acquisition and analysis. PTF provided satellite images and TRR the geological expertise. All authors contributed to the writing.

Acknowledgements. We thank the British Antarctic Survey (BAS) Operations Team and Air Unit for facilitating the remote sensing of the PICS site.

https://doi.org/10.5194/tc-2022-144
Preprint. Discussion started: 21 July 2022

References

Aitkenhead, N.: An Ice Caldera in North-east Graham Land, British Antarctic Survey Bulletin, 1, 9-15, 1963.
Arnold, E., Leuschen, C., Rodriguez-Morales, F., Li, J., Paden, J., Hale, R., & Keshmiri, S. : CReSIS airborne radars and platforms for ice and snow sounding, Annals of Glaciology, 61(81), 58-67, doi:10.1017/aog.2019.37, 2020.
Banwell, A. F., Datta, R. T., Dell, R. L., Moussavi, M., Brucker, L., Picard, G., Shuman, C. A., and Stevens, L. A.: The 32-year record-high surface melt in 2019/2020 on the northern George VI Ice Shelf, Antarctic Peninsula, The Cryosphere, 15, 909-925, 10.5194/tc-15-909-2021, 2021.
Bartholomew, I., Nienow, P., Sole, A., Mair, D., Cowton, T., and King, M. A.: Short-term variability in Greenland Ice Sheet motion forced by time-varying meltwater drainage: Implications for the relationship between subglacial drainage system behavior and ice velocity, Journal of Geophysical Research: Earth Surface, 117, https://doi.org/10.1029/2011JF002220, 2012.
Benn, D. and Evans, D. J. A.: Glaciers and Glaciation, 2nd Routledge, https://doi.org/10.4324/9780203785010, 2010.
Bindschadler, R., Scambos, T. A., Rott, H., Skvarca, P., and Vornberger, P.: Ice dolines on Larsen Ice Shelf, Antarctica, Annals of Glaciology, 34, 283-290, 10.3189/172756402781817996, 2002.
Björnsson, H.: Subglacial lakes and jökulhlaups in Iceland, Global and Planetary Change, 35, 255-271, https://doi.org/10.1016/S0921-8181(02)00130-3, 2003.
Boronina, A., Popov, S., Pryakhina, G., Chetverova, A., Ryzhova, E., and Grigoreva, S.: Formation of a large ice depression on Dålk Glacier (Larsemann Hills, East Antarctica) caused by the rapid drainage of an englacial cavity, Journal of Glaciology, 67, 1121-1136, 10.1017/jog.2021.58, 2021.
Boxall, K., Christie, F. D. W., Willis, I. C., Wuite, J., and Nagler, T.: Seasonal land ice-flow variability in the Antarctic Peninsula, The Cryosphere Discuss., 2022, 1-37, 10.5194/tc-2022-55, 2022.
Capps, D. M., Rabus, B., Clague, J. J., and Shugar, D. H.: Identification and characterization of alpine subglacial lakes using interferometric synthetic aperture radar (InSAR): Brady Glacier, Alaska, USA, Journal of Glaciology, 56, 861-870, 10.3189/002214310794457254, 2010.
Carrivick, J. L., Sutherland, J. L., Huss, M., Purdie, H., Stringer, C. D., Grimes, M., James, W. H. M., and Lorrey, A. M.: Coincident evolution of glaciers and ice-marginal proglacial lakes across the Southern Alps, New Zealand: Past, present and future, Global and Planetary Change, 103792, https://doi.org/10.1016/j.gloplacha.2022.103792, 2022.
Clarke, G. K. C.: Hydraulics of subglacial outburst floods: new insights from the Spring–Hutter formulation, Journal of Glaciology, 49, 299-313, 10.3189/172756503781830728, 2003.
Cooper, A. P. R.: Historical observations of Prince Gustav Ice Shelf, Polar Record, 33, 285-294, 10.1017/S0032247400025389, 1997.
DeConto, R. M., Pollard, D., Alley, R. B., Velicogna, I., Gasson, E., Gomez, N., Sadai, S., Condron, A., Gilford, D. M., Ashe, E. L., Kopp, R. E., Li, D., and Dutton, A.: The Paris Climate Agreement and future sea-level rise from Antarctica, Nature, 593, 83-89, 10.1038/s41586-021-03427-0, 2021.
Francelino, M. R., Schaefer, C., Skansi, M. d. L. M., Colwell, S., Bromwich, D. H., Jones, P., King, J. C., Lazzara, M. A., Renwick, J., Solomon, S., Brunet, M., and Cerveny, R. S.: WMO Evaluation of Two Extreme High Temperatures Occurring in February 2020 for the Antarctic Peninsula Region, Bulletin of the American Meteorological Society, 102, E2053-E2061, 10.1175/bams-d-21-0040.1, 2021.
Glen, J. W.: The Stability of Ice-Dammed Lakes and other Water-Filled Holes in Glaciers, Journal of Glaciology, 2, 316-318, 10.3189/S0022143000025132, 1954.
Hodgson, D. A., Roberts, S. J., Bentley, M. J., Carmichael, E. L., Smith, J. A., Verleyen, E., Vyverman, W., Geissler, P., Leng, M. J., and Sanderson, D. C. W.: Exploring former subglacial Hodgson Lake. Paper II: Palaeolimnology, Quaternary Science Reviews, 28, 2310-2325, doi:10.1016/j.quascirev.2009.04.014, 2009a.
Hodgson, D. A., Roberts, S. J., Bentley, M. J., Smith, J. A., Johnson, J. S., Verleyen, E., Vyverman, W., Hodson, A. J., Leng, M. J., Cziferszky, A., Fox, A. J., and Sanderson, D. C. W.: Exploring former subglacial Hodgson Lake. Paper I: Site description, geomorphology and limnology, Quaternary Science Reviews, 28, 2295-2309, doi:10.1016/j.quascirev.2009.04.011, 2009b.
Howat, I. M., Porter, C., Smith, B. E., Noh, M. J., and Morin, P.: The Reference Elevation Model of Antarctica, The Cryosphere, 13, 665-674, 10.5194/tc-13-665-2019, 2019.
Kashani, A. G., Olsen, M. J., Parrish, C. E., and Wilson, N.: A Review of LIDAR Radiometric Processing: From Ad Hoc Intensity Correction to Rigorous Radiometric Calibration, Sensors (Basel), 15, 28099-28128, 10.3390/s151128099, 2015.
Koerner, R. M.: An ice caldera near Hope Bay, Trinity Peninsula, Graham Land, British Antarctic Survey Bulletin, 37-39, 1964.

https://doi.org/10.5194/tc-2022-144
Preprint. Discussion started: 21 July 2022

Lai, C.-Y., Kingslake, J., Wearing, M. G., Chen, P.-H. C., Gentine, P., Li, H., Spergel, J. J., and van Wessem, J. M.: Vulnerability of Antarctica's ice shelves to meltwater-driven fracture, Nature, 584, 574-578, 10.1038/s41586-020-2627-8, 2020.

Lenaerts, J. T. M., Lhermitte, S., Drews, R., Ligtenberg, S. R. M., Berger, S., Helm, V., Smeets, C. J. P. P., Broeke, M. R. van d., van de Berg, W. J., van Meijgaard, E., Eijkelboom, M., Eisen, O., and Pattyn, F.: Meltwater produced by wind–albedo interaction stored in an East Antarctic ice shelf, Nature Climate Change, 7, 58-62, 10.1038/nclimate3180, 2017.

Livingstone, S. J., Sole, A. J., Storrar, R. D., Harrison, D., Ross, N., and Bowling, J.: Brief communication: Subglacial lake drainage beneath Isunguata Sermia, West Greenland: geomorphic and ice dynamic effects, The Cryosphere, 13, 2789-2796, 10.5194/tc-13-2789-2019, 2019.

Livingstone, S. J., Li, Y., Rutishauser, A., Sanderson, R. J., Winter, K., Mikucki, J. A., Björnsson, H., Bowling, J. S., Chu, W., Dow, C. F., Fricker, H. A., McMillan, M., Ng, F. S. L., Ross, N., Siegert, M. J., Siegfried, M., and Sole, A. J.: Subglacial lakes and their changing role in a warming climate, Nature Reviews Earth & Environment, 3, 106-124, 10.1038/s43017-021-00246-9, 2022.

Magnússon, E., Rott, H., Björnsson, H., and Pálsson, F.: The impact of jökulhlaups on basal sliding observed by SAR interferometry on Vatnajökull, Iceland, Journal of Glaciology, 53, 232-240, 10.3189/172756507782202810, 2007.

Pearce, D. A., Hodgson , D. A., Thorne, M. A. S., Burns, G., and Cockell, C. S.: Preliminary Analysis of Life within a Former Subglacial Lake Sediment in Antarctica, Diversity, 5, 680-702; doi:610.3390/d5030680, 2013.

Perren, B. B., Hodgson, D. A., Roberts, S. J., Sime, L., Van Nieuwenhuyze, W., Verleyen, E., and Vyverman, W.: Southward migration of the Southern Hemisphere westerly winds corresponds with warming climate over centennial timescales, Communications Earth & Environment, 1, 58, 10.1038/s43247-020-00059-6, 2020.

Reynolds, H. I., Gudmundsson, M. T., Högnadóttir, T., and Axelsson, G.: Changes in Geothermal Activity at Bárdarbunga, Iceland, Following the 2014–2015 Caldera Collapse, Investigated Using Geothermal System Modeling, Journal of Geophysical Research: Solid Earth, 124, 8187-8204, https://doi.org/10.1029/2018JB017290, 2019.

Rignot, E., Mouginot, J., Scheuchl, B., Broeke, M. v. d., Wessem, M. J. v., and Morlighem, M.: Four decades of Antarctic Ice Sheet mass balance from 1979–2017, Proceedings of the National Academy of Sciences, 116, 1095-1103, doi:10.1073/pnas.1812883116, 2019.

Scambos, T. A., Berthier, E., and Shuman, C. A.: The triggering of subglacial lake drainage during rapid glacier drawdown: Crane Glacier, Antarctic Peninsula, Annals of Glaciology, 52, 74-82, 10.3189/172756411799096204, 2011.

Smellie, J. L. and Hole, M. J.: Chapter 4.1a Antarctic Peninsula: volcanology, Geological Society, London, Memoirs, 55, 305-325, 10.1144/m55-2018-59, 2021.

Smellie, J. L., Pankhurst, R. J., Hole, M. J., and Thomson, J. W.: Age, distribution and eruptive conditions of late Cenozoic alkaline volcanism in the Antarctic Peninsula and eastern Ellsworth Land: a review, British Antarctic Survey Bulletin, 21-49, 1988.

Smith, A. M., Woodward, J., Ross, N., Bentley, M. J., Hodgson, D. A., Siegert, M. J., and King, E. C.: Evidence for the long-term sedimentary environment in an Antarctic subglacial lake, Earth and Planetary Science Letters, 504, 139-151, https://doi.org/10.1016/j.epsl.2018.10.011, 2018.

Trusel, L. D., Frey, K. E., Das, S. B., Karnauskas, K. B., Kuipers Munneke, P., van Meijgaard, E., and van den Broeke, M. R.: Divergent trajectories of Antarctic surface melt under two twenty-first-century climate scenarios, Nature Geoscience, 8, 927-932, 10.1038/ngeo2563, 2015.

Tuckett, P. A., Ely, J. C., Sole, A. J., Livingstone, S. J., Davison, B. J., Melchior van Wessem, J., and Howard, J.: Rapid accelerations of Antarctic Peninsula outlet glaciers driven by surface melt, Nature Communications, 10, 4311, 10.1038/s41467-019-12039-2, 2019.

Turner, J., Lu, H., White, I., King, J. C., Phillips, T., Hosking, J. S., Bracegirdle, T. J., Marshall, G. J., Mulvaney, R., and Deb, P.: Absence of 21st century warming on Antarctic Peninsula consistent with natural variability, Nature, 535, 411-415, 10.1038/nature18645, 2016.

Warner, R. C., Fricker, H. A., Adusumilli, S., Arndt, P., Kingslake, J., and Spergel, J. J.: Rapid Formation of an Ice Doline on Amery Ice Shelf, East Antarctica, Geophysical Research Letters, 48, e2020GL091095, https://doi.org/10.1029/2020GL091095, 2021.

https://doi.org/10.5194/tc-2022-144
Preprint. Discussion started: 21 July 2022

Figures.

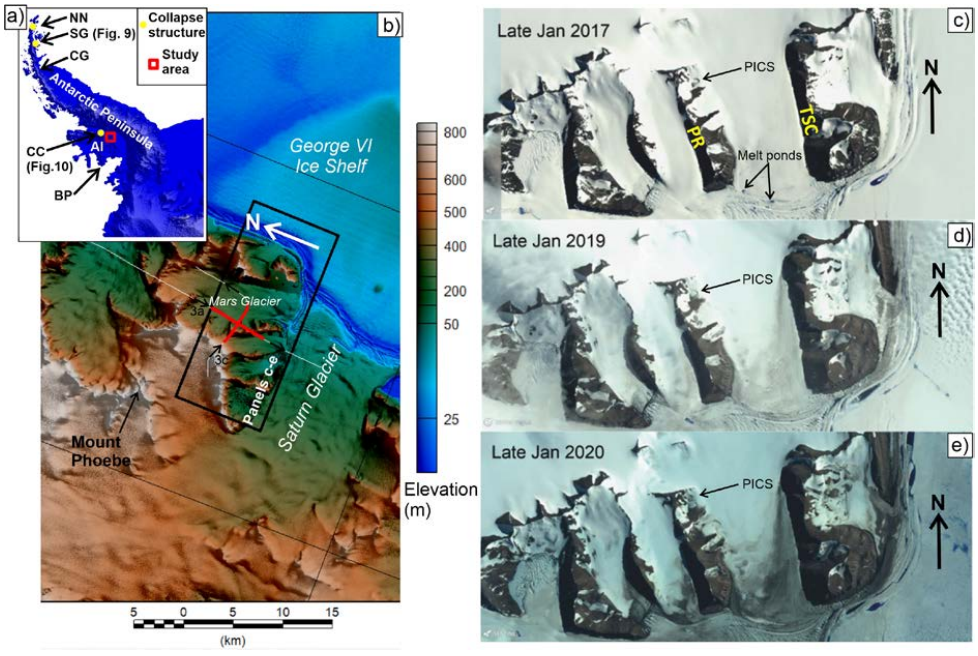

Figure 1: Location of Phobos Ice Collapse Structure (PICS). a) Location of Alexander Island (AI) and the PICS (red box) on the Antarctic Peninsula. Yellow dots mark other ice collapse structures at Nobby Nunatak (NN), and Sjögren Glacier (SG) in the northern Antarctic Peninsula (Aitkinhead, 1963; Keorner 1964) and in the southern Antarctic Peninsula at Callisto Cliffs (CC) on Alexander Island. BP marks the location of the Beethoven Peninsula volcanic field. CG marks Crane Glacier where satellite altimetry indicated a draining subglacial lake (Scambos et al., 2011). b) REMA digital elevation model (Howat et al., 2019). Thin white lines mark 2019 LiDAR flights over the PICS. Black arrows mark flight direction, and red flight segments locate radar sections in Fig. 4. Black box locates Sentinel satellite images. c-e) Satellite images showing persistence of the PICS from 2017 to 2020. TSC and PR indicate Two Step Cliffs and Phobos Ridge respectively. Note evidence for extensive surface meltwater on George VI Ice Shelf and the terminus of Mars Glacier in all years, and the increase in dust on the surface of the glacier in 2019 and 2020. Copernicus Sentinel data 2021, processed by ESA.

https://doi.org/10.5194/tc-2022-144
Preprint. Discussion started: 21 July 2022

The Cryosphere
Discussions
Open Access
EGU

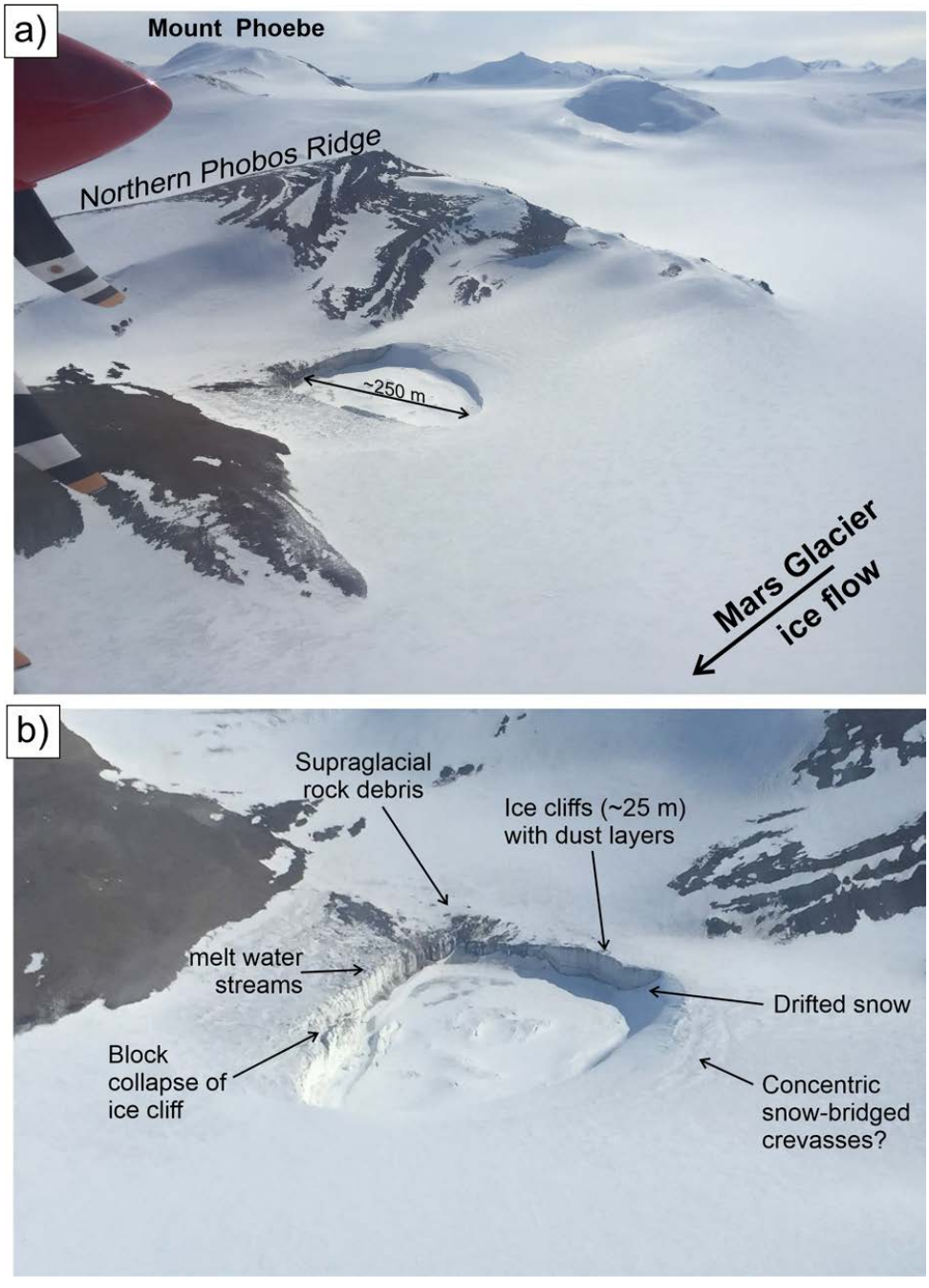

Figure 2: Oblique aerial photographs of PICS structure in 2018. a) View looking northwest from Mars Glacier towards Phobos Ridge and Mount Phoebe beyond. b) Closer view looking approximately southwest. Author photographs (DH).

https://doi.org/10.5194/tc-2022-144
Preprint. Discussion started: 21 July 2022

The Cryosphere
Discussions
Open Access
EGU

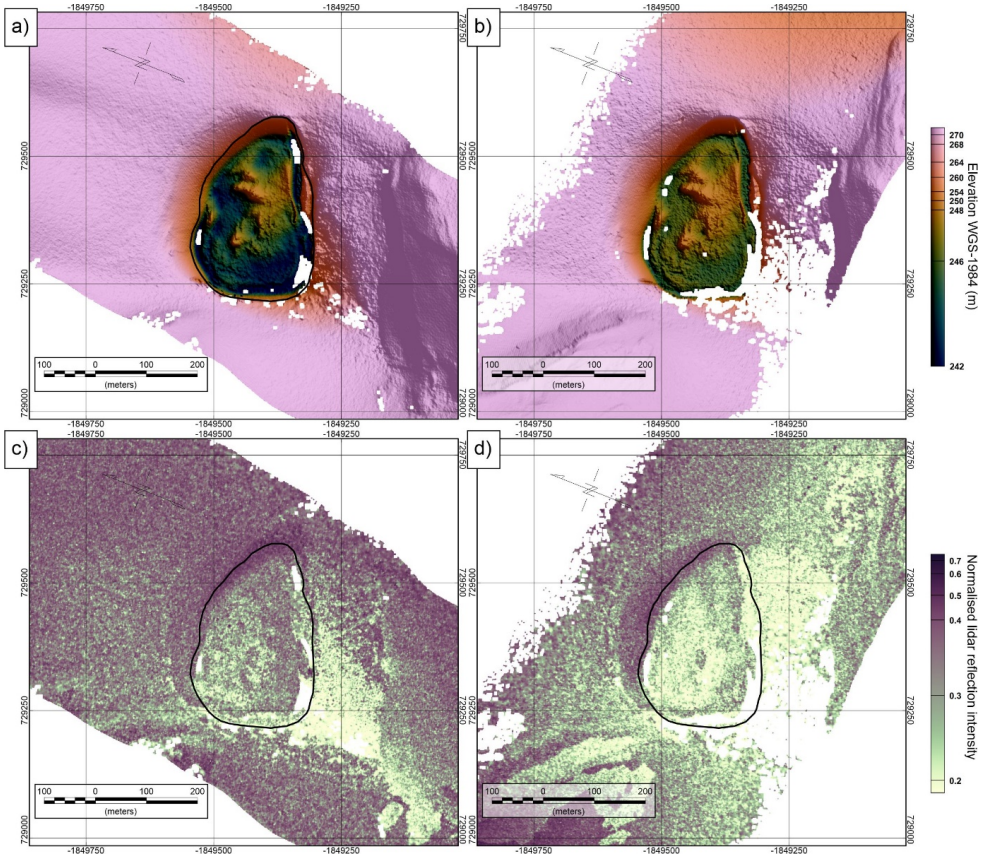

Figure 3: LiDAR imaging of PICS. a) LiDAR elevation from flight on the 22nd Dec 2019. Thin black line marks peak in maximum horizontal gradient of elevation locating ice cliffs bounding the PICS. b) LiDAR surface elevation from flight on 30th December. c) LiDAR reflection intensity from 22nd Dec 2019 flight. d) LiDAR reflection intensity from 30th Dec 2019 flight.

https://doi.org/10.5194/tc-2022-144
Preprint. Discussion started: 21 July 2022

2019 flight. d) LiDAR reflection intensity from 30th Dec 2019 flight.

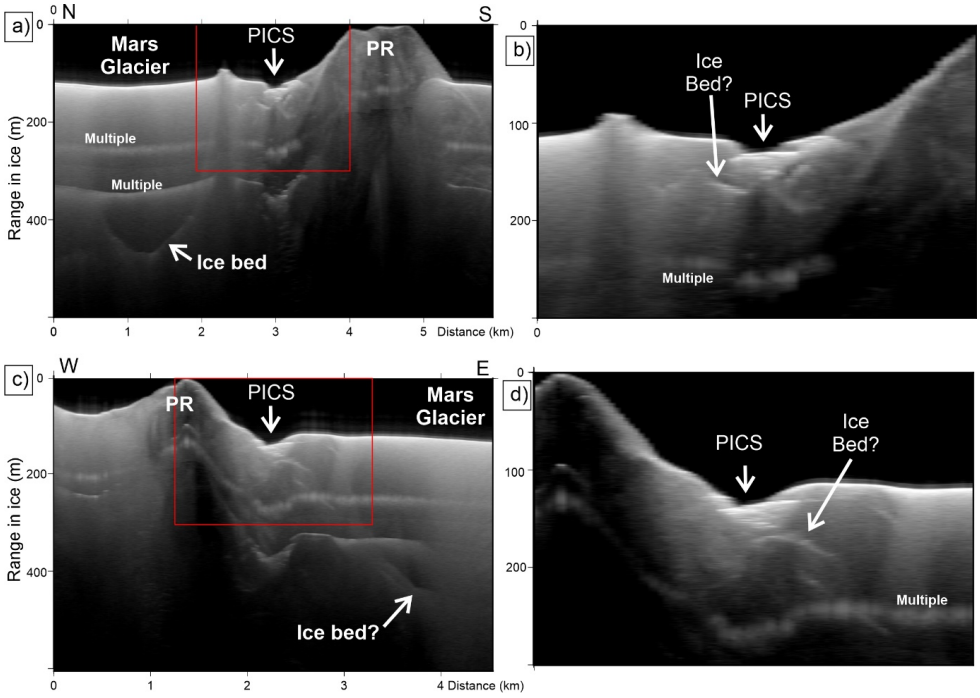

Figure 4: Radar sections located as red lines in Figure 1. Vertical scale is relative range in ice. Image brightness indicates strength of the returned reflection, on a log scale. a) North to South section. Note ice bed reflection ~400 m below the surface beneath Mars Glacier. PR marks Phobos Ridge. b) Detail over PICS. Note potential ice-bed reflection between 35 and 50 m beneath the ice surface. c) West to East section. d) Detail of PICS on West to East section.

https://doi.org/10.5194/tc-2022-144
Preprint. Discussion started: 21 July 2022

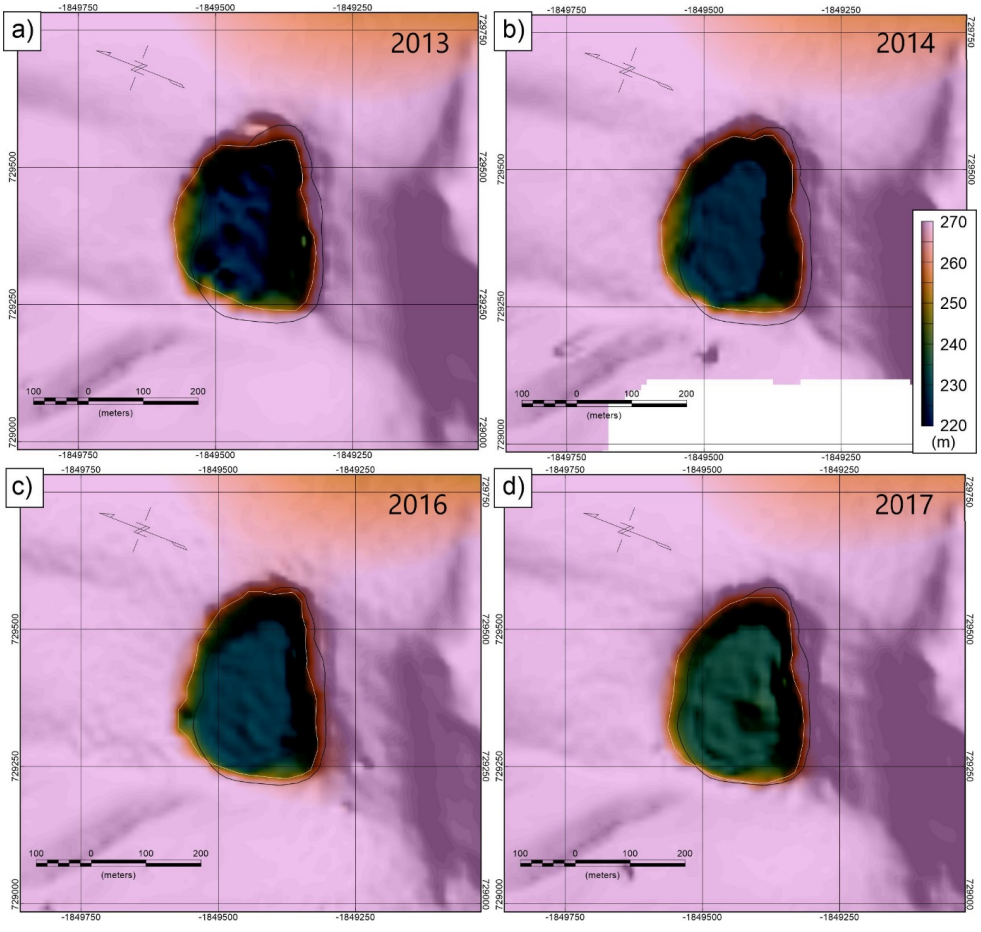

Figure 5: REMA strip DEM's over the PICS. All DEM's are shown with a uniform colour scale. Black line outlies the PICS as observed in 2019 from maximum horizontal gradient of 2019 LiDAR elevation data. White line shows edge of PICS from maximum horizontal gradient of strip DEM. a) 2013 DEM. b) 2014 DEM. c) 2016 DEM. e) 2017 DEM. Note deep and more rugged floor to the PICS in 2013.

https://doi.org/10.5194/tc-2022-144
Preprint. Discussion started: 21 July 2022

The Cryosphere
Discussions
Open Access
EGU

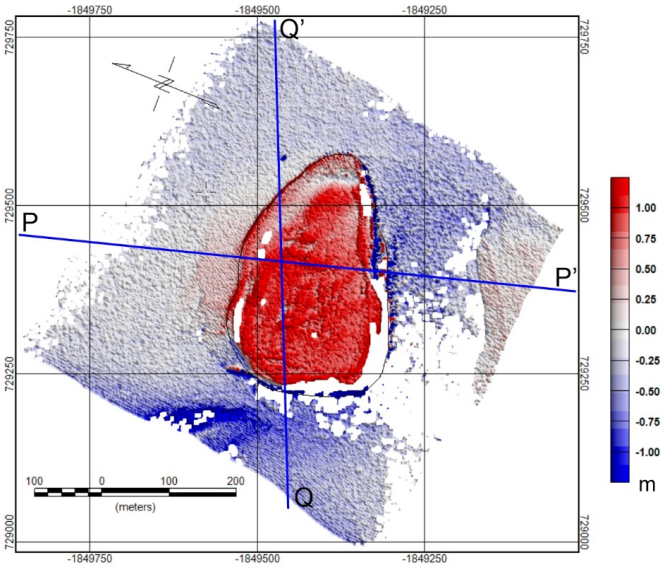

Figure 6: Change in elevation between 22nd and 30th December 2019. Blue lines locate sections shown in Fig. 7.

https://doi.org/10.5194/tc-2022-144
Preprint. Discussion started: 21 July 2022

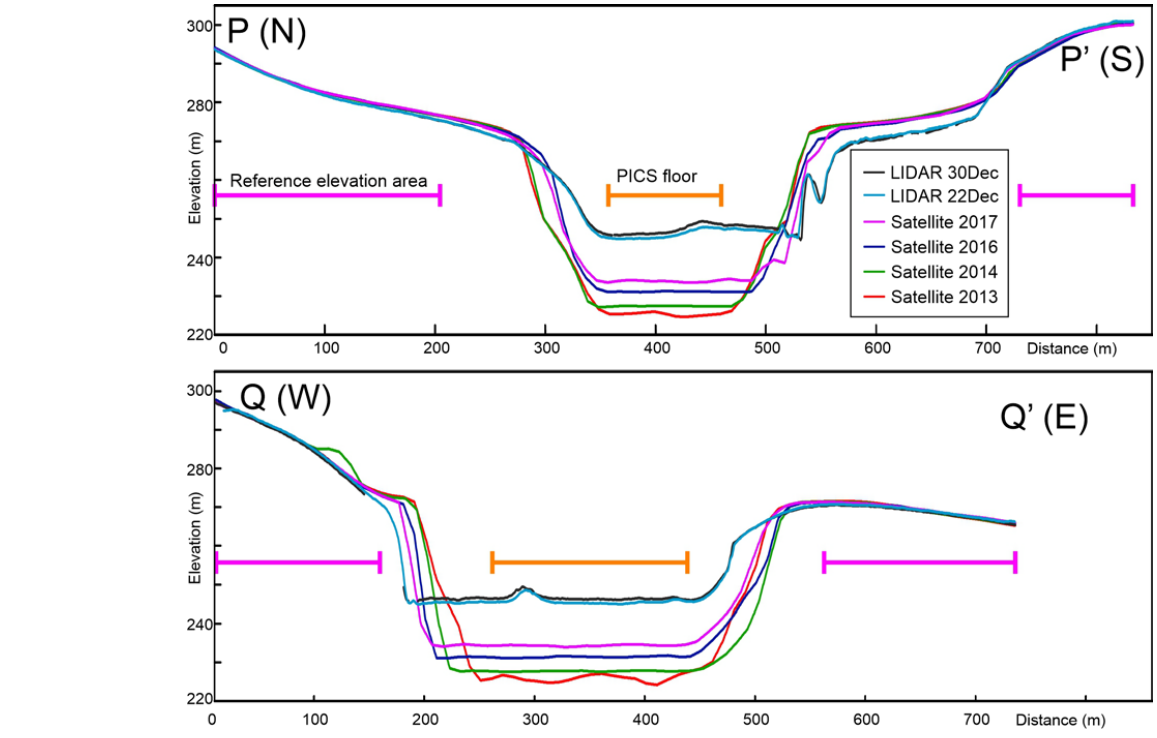

Figure 7: Profiles of surface elevation over the PICS structure. Locations shown in in Fig. 6. Reference elevation areas were used to calibrate the mean vertical shift applied to the satellite derived REMA strip DEM elevation values (2013 to 2017). LiDAR profiles are un-adjusted. PICS floor region was used to calculate the average floor elevation plotted in Fig. 8.

https://doi.org/10.5194/tc-2022-144
Preprint. Discussion started: 21 July 2022

The Cryosphere
Discussions
Open Access
EGU

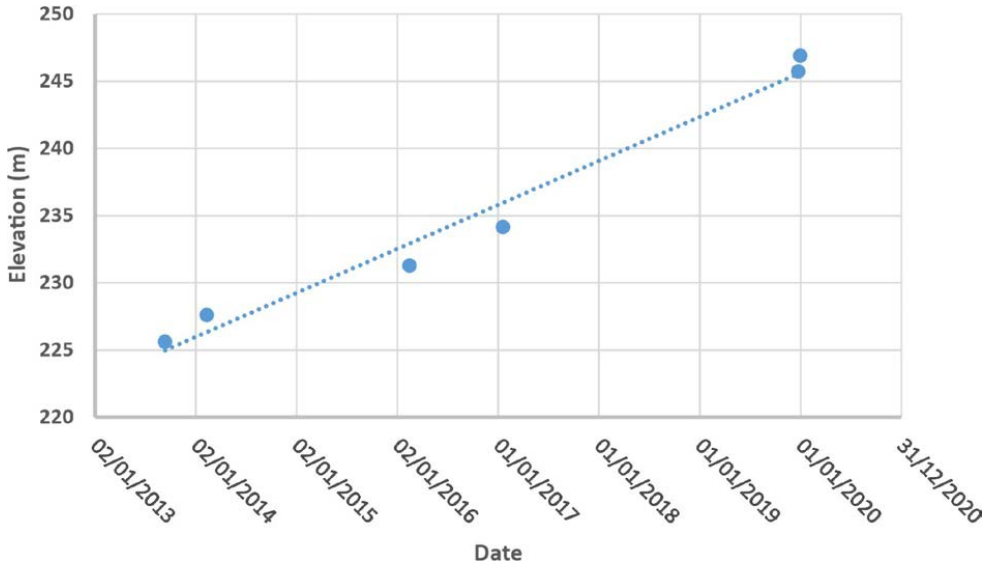

Figure 8: Average elevation of PICS floor with time. Slope of best-fit line indicates an average increase in the elevation of the PICS floor by 3.28 m per year.

https://doi.org/10.5194/tc-2022-144
Preprint. Discussion started: 21 July 2022

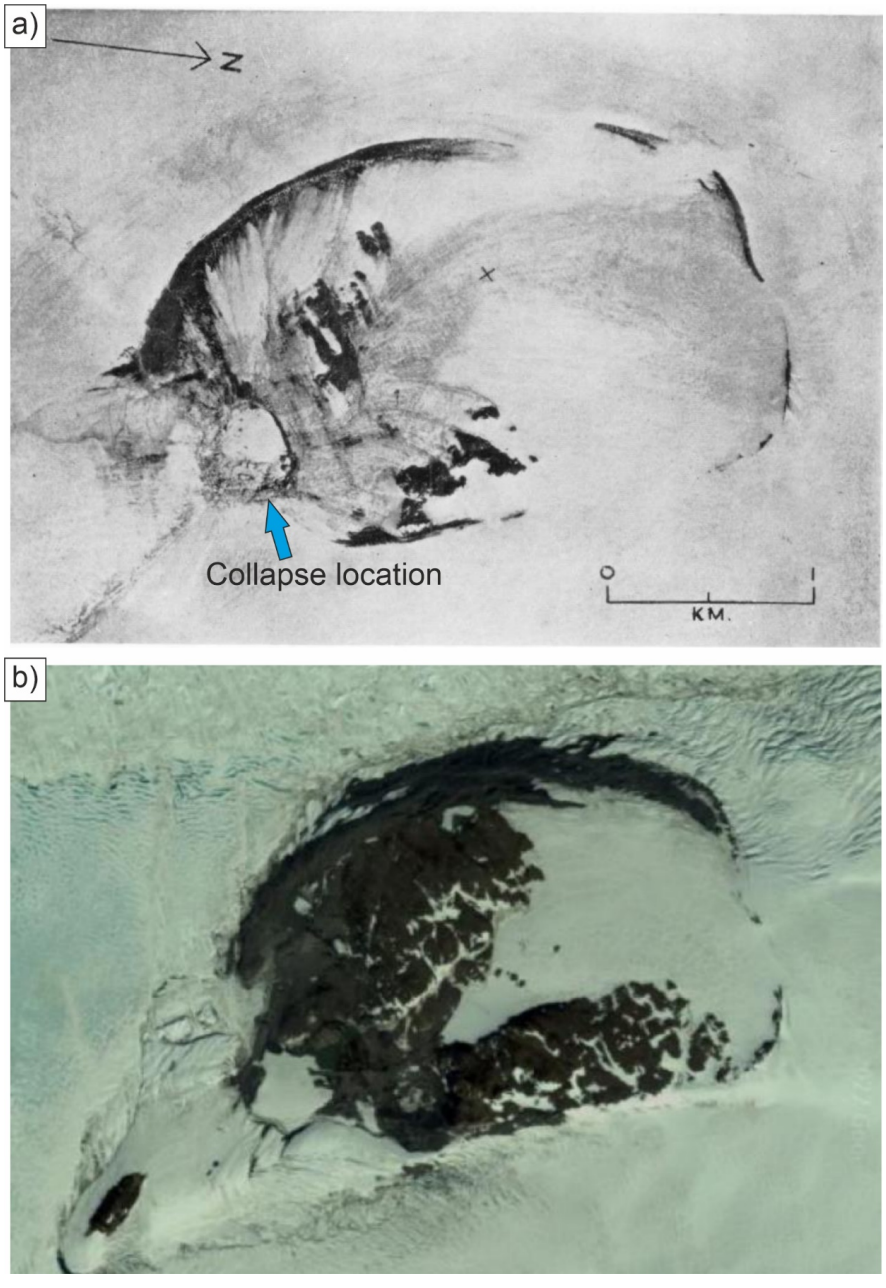

Figure 9: Ice collapse structure on the northern Antarctic Peninsula (reproduced from Aitkenhead, 1963). a) Aerial photograph from 1957, with blue arrow marking the location of the collapse (Aitkenhead, 1963). b) Recent 2015 satellite image of the feature from Google Earth (Imagery date 1/1/15, Maxar Technologies).

https://doi.org/10.5194/tc-2022-144
Preprint. Discussion started: 21 July 2022

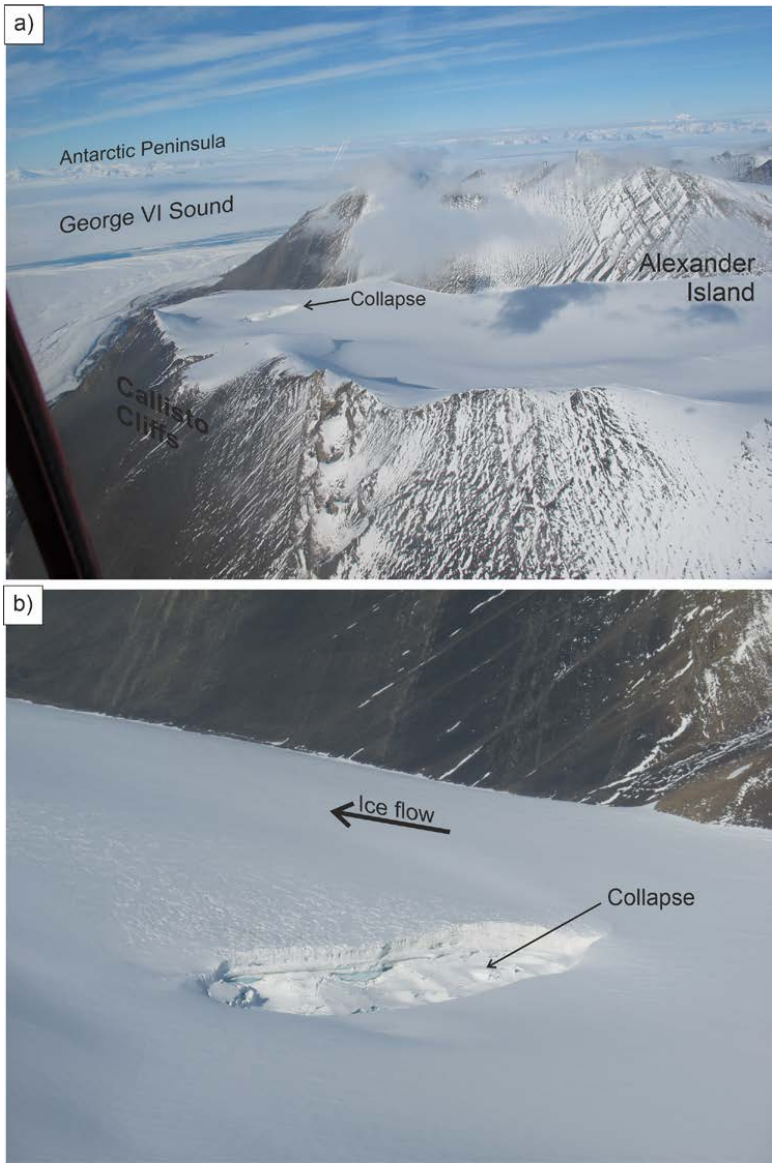

Figure 10. Ice collapse structure at Callisto Cliffs on Alexander Island. a) View looking approximately southeast towards the adjacent George VI Sound. First observed in March 2022. b) Zoom on collapse structure. Note extensive crevassing on the down-stream side of the structure which may reflect partial collapse of the roof of the outlet channel/channels.

END